

Early Galaxies and Early Dark Energy: A Unified Solution to the Hubble Tension and Puzzles of Massive Bright Galaxies revealed by JWST

Xuejian Shen,^{1*} Mark Vogelsberger,^{1,2} Michael Boylan-Kolchin,³ Sandro Tacchella,^{4,5} Rohan P. Naidu^{1†}

¹ Department of Physics & Kavli Institute for Astrophysics and Space Research, Massachusetts Institute of Technology, Cambridge, MA 02139, USA

² The NSF AI Institute for Artificial Intelligence and Fundamental Interactions, Massachusetts Institute of Technology, Cambridge, MA 02139, USA

³ Department of Astronomy, The University of Texas at Austin, 2515 Speedway Stop C1400, Austin, TX 78712, USA

⁴ Kavli Institute for Cosmology, University of Cambridge, Madingley Road, Cambridge, CB3 0HA, UK

⁵ Cavendish Laboratory, University of Cambridge, 19 JJ Thomson Avenue, Cambridge, CB3 0HE, UK

Accepted XXX. Received YYY; in original form ZZZ

ABSTRACT

JWST has revealed a large population of ultra-violet (UV)-bright galaxies at $z \gtrsim 10$ and possibly overly massive galaxies at $z \gtrsim 7$, challenging standard galaxy formation models in the Λ CDM cosmology. We use an empirical galaxy formation model to explore the potential of alleviating these tensions through an Early Dark Energy (EDE) model, originally proposed to solve the Hubble tension. Our benchmark model demonstrates excellent agreement with the UV luminosity functions (UVLFs) at $4 \lesssim z \lesssim 10$ in both Λ CDM and EDE cosmologies. In the EDE cosmology, the UVLF measurements at $z \approx 12$ based on spectroscopically confirmed galaxies exhibit no tension with the benchmark model. Photometric constraints at $12 \lesssim z \lesssim 16$ can be fully explained within EDE via either moderately increased star formation efficiencies ($\epsilon_* \sim 3 - 10\%$ at $M_{\text{halo}} \sim 10^{10.5} M_{\odot}$) or enhanced UV variabilities ($\sigma_{\text{UV}} \sim 0.8 - 1.3$ mag at $M_{\text{halo}} \sim 10^{10.5} M_{\odot}$) that are within the scatter of hydrodynamical simulation predictions. A similar agreement is difficult to achieve in Λ CDM, especially at $z \gtrsim 14$, where the required σ_{UV} exceeds the maximum value seen in simulations. Furthermore, the implausibly large cosmic stellar mass densities inferred from some JWST observations are no longer in tension with cosmology when the EDE is considered. Our findings highlight EDE as an intriguing unified solution to a fundamental problem in cosmology and the recent tensions raised by JWST observations. Data at the highest redshifts reached by JWST ($z \sim 14 - 16$) will be crucial for differentiating modified galaxy formation physics from new cosmological physics.

Key words: galaxies: high-redshift – galaxies: formation – galaxies: evolution – cosmology: theory – dark energy

1 INTRODUCTION

The James Webb Space Telescope (JWST) has opened a new window for studying galaxy formation and evolution within the first ~ 500 Myr ($z \gtrsim 10$) of the history of the Universe. Numerous photometric drop-out galaxy candidates at $z \gtrsim 9$ have been unveiled by the JWST/NIRCam imaging datasets (e.g. Naidu et al. 2022b; Castellano et al. 2022; Finkelstein et al. 2022; Adams et al. 2023b; Atek et al. 2023; Bouwens et al. 2023b; Donnan et al. 2023; Harikane et al. 2023; Robertson et al. 2023a; Yan et al. 2023; Hainline et al. 2024), with unusually bright galaxy candidates revealed at $z \approx 16$ (e.g. Harikane et al. 2023). Among these galaxies, seven of the $z \gtrsim 12$ candidates have already been spectroscopically confirmed in the JADES (Robertson et al. 2023a; Curtis-Lake et al. 2023; D’Eugenio et al. 2023; Carniani et al. 2024), GLASS (Bakx et al. 2023; Castellano et al. 2024; Zavala et al. 2024), and UNCOVER survey (Wang et al. 2023; Fujimoto et al. 2023).

The rest-frame UV luminosity functions (UVLFs) determined using JWST-identified galaxies show surprisingly little evolution at the

bright end beyond $z \approx 10$ (e.g. Harikane et al. 2023; Finkelstein et al. 2023b) and differ substantially from the extrapolation of results derived from previous Hubble Space Telescope (HST) observations. Meanwhile, the number densities of UV-bright galaxies at $z \gtrsim 10$ inferred from these observations are in tension with predictions of the majority of the theoretical models (developed before JWST observations, as summarized in e.g. Finkelstein et al. 2023a,b). This includes empirical models (e.g. Tacchella et al. 2013; Mason et al. 2015; Sun & Furlanetto 2016; Tacchella et al. 2018; Behroozi et al. 2020), semi-analytical galaxy formation models (e.g. Dayal et al. 2014, 2019; Cowley et al. 2018; Yung et al. 2019; Mauerhofer & Dayal 2023; Yung et al. 2024b), and cosmological hydrodynamic simulations (e.g. Davé et al. 2019; Vogelsberger et al. 2020; Haslbauer et al. 2022; Kannan et al. 2022, 2023; Wilkins et al. 2023b,a). This discrepancy is largely based on the photometrically-selected galaxy candidates, which could be contaminated by low-redshift interlopers (e.g. Fujimoto et al. 2022; Zavala et al. 2023; Naidu et al. 2022a). However, there has been a good agreement between the photometric and spectroscopic redshifts for the spectroscopically confirmed galaxies so far (e.g. Finkelstein et al. 2023a). The pure spectroscopic constraints of the UVLF (e.g. Harikane et al. 2024b,a) also yield broadly consistent results with the photometric estimates.

* E-mail: xuejian@mit.edu

† NASA Hubble Fellow

Such discrepancies are not completely unexpected, as many of these galaxy formation models were calibrated based on low-redshift observations, and qualitative differences in galaxy formation and evolution could exist in the extremely dense and low-metallicity environment of cosmic dawn (e.g. [Dekel et al. 2023](#); [Ceverino et al. 2024](#); [Lu et al. 2024](#)). Many physical interpretations of the tension have already been discussed in the literature, including but not limited to: (1) a substantially higher star-formation efficiency (SFE) in massive galaxies at $z \gtrsim 10$ (e.g. [Li et al. 2023](#); [Ceverino et al. 2024](#)) potentially due to a feedback-free/failure regime (e.g. [Fall et al. 2010](#); [Thompson & Krumholz 2016](#); [Grudić et al. 2018](#); [Dekel et al. 2023](#); [Menon et al. 2024](#)); (2) a top-heavy stellar initial mass function (IMF; e.g. [Inayoshi et al. 2022](#); [Yung et al. 2024b](#); [Cueto et al. 2024](#); [Trinca et al. 2024](#); [Wang et al. 2024b](#); [Lu et al. 2024](#); [Ventura et al. 2024](#)) to increase the light-to-mass ratios of the stellar population, although increased feedback-to-mass ratios could cancel this effect (e.g. [Cueto et al. 2024](#)); (3) negligible dust attenuation ([Ferrara et al. 2023a](#), but depends on the galaxy formation model used, as in some models, even the no-dust prediction is in tension with observations.); (4) UV radiation contributed by non-stellar sources, e.g. accreting stellar-mass black holes, quasars/active galactic nuclei (AGN; e.g. [Inayoshi et al. 2022](#); [Trinca et al. 2024](#); [Hegde et al. 2024](#)) and see an observational case study of GN-z11 ([Tacchella et al. 2023b](#)).

The solutions above focus on enhancing the UV photon yield in high-redshift galaxies. An alternative and orthogonal solution involves variability/stochasticity of galaxy UV luminosity at fixed halo mass (e.g. [Mason et al. 2023](#); [Mirocha & Furlanetto 2023](#); [Shen et al. 2023](#); [Sun et al. 2023a](#); [Kravtsov & Belokurov 2024](#); [Gelli et al. 2024](#)) without changing the median UV photon yield of galaxies. In this scenario, the bright end of the UVLF is populated by a large number of low-mass haloes with upscattered UV brightness. In [Shen et al. \(2023\)](#), a constant UV variability of $\sigma_{UV} \approx 1.5$ (2.5) mag is suggested to reconcile observations at $z \approx 12$ (16). The σ_{UV} value is reduced to $\approx 1 - 1.3$ (2) mag with more detailed modelling of the bursty star-formation histories of galaxies ([Kravtsov & Belokurov 2024](#)). [Gelli et al. \(2024\)](#) considered the halo mass-dependence of σ_{UV} and found that the $z \approx 12$ observations can be reconciled with theoretical models without modifications to $\sigma_{UV}(M_{\text{halo}})$ at lower redshifts, but the $z \gtrsim 14$ results remain challenging.

Observational signatures of large burstiness of star-formation in high-redshift galaxies have been found (e.g. [Ciesla et al. 2023](#); [Cole et al. 2023](#); [Endsley et al. 2023a](#); [Looser et al. 2023](#); [Tacchella et al. 2023a](#); [Dressler et al. 2024](#); [Helton et al. 2024](#)) with a potential qualitative transition around $z \approx 10$. The major source of this variability could come from the bursty star-formation in low-mass, high-redshift galaxies, often seen in cosmological zoom-in simulations with advanced models for star-formation and feedback in the interstellar medium (ISM; e.g. [Hopkins et al. 2018](#); [Faucher-Giguère 2018](#); [Marinacci et al. 2019](#); [Sun et al. 2023a](#); [Katz et al. 2023](#)). Increased variability at $z \gtrsim 10$ could come from stochastic gas inflow (e.g. [Tacchella et al. 2020](#)), rapid star-formation in a feedback-failure regime (e.g. [Grudić et al. 2018](#); [Dekel et al. 2023](#); [Menon et al. 2024](#)), in massive star clusters due to Lyman-Werner radiation feedback in metal-poor environment (e.g. [Sugimura et al. 2024](#)), or due to highly clustered (in both space and time) feedback from a top-heavy IMF. Enhanced variability in clumpy, high-redshift galaxies could also result indirectly from the limited statistics of star-forming regions and the increased sampling noises.

However, the aforementioned ideas all assume the standard Λ CDM cosmology. While this model has been singularly successful at explaining a variety of cosmological observations across a range of length scales and cosmic epochs, questions still remain about whether

it is a complete (albeit phenomenological) description of the evolution of the Universe. In particular, a persistent discrepancy between inferences of the current expansion rate of the Universe based on modeling anisotropies in the Cosmic Microwave Background (CMB; e.g. [Planck Collaboration et al. 2020](#)) and directly measuring the expansion locally (e.g. [Riess et al. 2022](#)) — the so-called “Hubble tension” (see [Abdalla et al. 2022](#) for a review) — has prompted a flurry of activity aimed at understanding how to preserve Λ CDM’s successes while resolving this tension (see [Di Valentino et al. 2021](#) for a review).

Given the abundance of precision cosmological data now available, modifications to the standard Λ CDM that do not conflict with observations are surprisingly difficult to realize. The “least unlikely” type of modification that is allowed ([Knox & Millea 2020](#)) increases the expansion rate of the Universe before recombination. This modification decreases the physical sound horizon measured by the CMB, requiring an attendant decrease in the distance to the last scattering that is obtained through an increase in H_0 . One possible mechanism for achieving this increased expansion at early times is “Early Dark Energy” (EDE), where a new cosmological energy source with an equation of state similar to dark energy contributes $\sim 10\%$ of the critical density at its time of maximal contribution ($z \sim 3000$; see [Poulin et al. 2023](#) for a recent review). In this work, we specifically explore a scalar field model of EDE, as proposed in [Karwal & Kamionkowski \(2016\)](#); [Poulin et al. \(2018, 2019\)](#); [Smith et al. \(2020\)](#) to solve the Hubble tension. As the EDE in this model decays rapidly after recombination and exerts negligible dynamical effects at late times, its primary influence on structure formation is through altered cosmological parameters, notably increasing both the amplitude A_s and spectral index n_s of primordial scalar fluctuations, and the physical matter density ω_{cdm} .

As a consequence of these changes in cosmological parameters, the halo and thus galaxy abundance are systematically enhanced at high redshifts (e.g. [Klypin et al. 2021](#); [Boylan-Kolchin 2023](#); [Forconi et al. 2024](#)), which has the potential to alleviate the UVLF tension discussed above. The enhanced halo abundance also has implications for another tension raised by JWST regarding potentially overly-massive galaxies at $z \gtrsim 5$ (e.g. [Labbé et al. 2023](#); [Akins et al. 2023](#); [Xiao et al. 2023](#); [de Graaff et al. 2024a](#); [Casey et al. 2024](#)). In some cases (e.g. [Labbé et al. 2023](#)), the implied cosmic stellar mass density exceeds the total mass budget of baryons in a Λ CDM universe ([Boylan-Kolchin 2023](#); [Lovell et al. 2023](#)). Despite the debated nature of these sources (e.g. [Endsley et al. 2023b](#); [Larson et al. 2022](#); [Kocevski et al. 2023](#); [Desprez et al. 2024](#); [Narayanan et al. 2024](#); [Wang et al. 2024b](#)), EDE offers an alternative way to alleviate this potential cosmological tension.

In this paper, we investigate the potential of EDE as a unified solution to the Hubble tension and the tensions regarding UV-bright and potentially overly massive galaxies raised by JWST. The paper is organized as follows: In Section 2, we introduce the EDE model and the calculation of dark matter halo mass functions as well as growth rates. In Section 3, we discuss the galaxy formation model and establish a median mapping between the halo mass function and galaxy UVLF. We then describe how we treat UV variability and its halo mass dependence. In Section 4, we present the results and discuss how EDE changes the landscape of UVLFs at $z \gtrsim 10$ and the stellar mass densities at $z \gtrsim 7$. In Section 5, we provide discussions and our conclusions.

Model	Λ CDM	EDE
$f_{\text{EDE}}(z_c)$	-	$0.179^{+0.047}_{-0.04}$
$\log_{10}(z_c)$	-	$3.528^{+0.028}_{-0.024}$
θ_1	-	$2.806^{+0.098}_{-0.093}$
m (10^{-28} eV)	-	4.38 ± 0.49
f (Mpl)	-	0.213 ± 0.035
H_0 [$\text{km s}^{-1} \text{Mpc}^{-1}$]	$67.81^{+0.64}_{-0.6}$	$74.83^{+1.9}_{-2.1}$
$100\omega_b$	$2.249^{+0.014}_{-0.013}$	$2.278^{+0.018}_{-0.02}$
ω_{cdm}	$0.1191^{+0.0014}_{-0.0015}$	$0.1372^{+0.0053}_{-0.0059}$
$10^9 A_s$	$2.092^{+0.035}_{-0.033}$	$2.146^{+0.041}_{-0.04}$
n_s	$0.9747^{+0.0046}_{-0.0047}$	$1.003^{+0.0091}_{-0.0096}$
S_8	0.821 ± 0.017	$0.829^{+0.017}_{-0.019}$
Ω_m	$0.309^{+0.009}_{-0.008}$	0.287 ± 0.009

Table 1. The best-fit $\pm 1\sigma$ errors of the cosmological parameters reconstructed in the Λ CDM and EDE models from the analysis of the ACT DR4 + SPT-3G+Planck TT650TEEE dataset combination in [Smith et al. \(2022\)](#). $f_{\text{EDE}}(z) \equiv \Omega_a(z)/\Omega_{\text{tot}}(z)$ is the fraction of energy density contributed by EDE. z_c is the critical redshift when EDE becomes dynamical. θ_1 is the initial field value before oscillation. m is the mass of the scalar field. f is the decaying constant of the field in unit of Planck scale (Mpl). H_0 is the Hubble constant at $z = 0$. $\omega_x \equiv \Omega_x h^2$, where $h \equiv H_0/100$. A_s and n_s are the normalization and power-law index of the primordial power spectrum. Ω_m is matter density. $S_8 \equiv \sigma_8(\Omega_m/0.3)^{1/2}$.

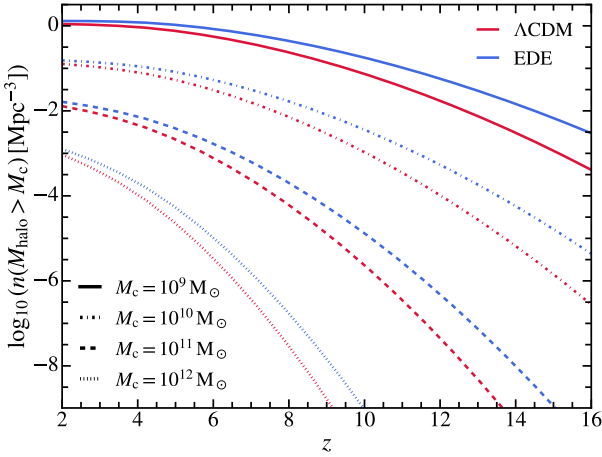


Figure 1. Number density of haloes above mass M_c versus redshift in the EDE and Λ CDM cosmology. We show results with $M_c = 10^9, 10^{10}, 10^{11}, 10^{12}$ with different types of lines. The halo counts in the EDE model are systematically enhanced at all mass scales at $z \geq 8$. However, the differences diminish at low redshifts.

2 COSMOLOGICAL MODEL

The EDE considered in this paper is a scalar field with an axion-like potential $V_n(\phi) \sim [1 - \cos(\phi/f)]^n$, where f is the decay constant of the field. These ultralight axion-like fields arise generically in string theory (e.g. [Svrcek & Witten 2006](#); [Arvanitaki et al. 2010](#); [Kamionkowski et al. 2014](#); [Marsh 2016](#)) and have intriguing cosmological implications for dark matter ([Marsh 2016](#)) and EDE ([Poulin et al. 2019](#)). The field is frozen at early times and acts as a cosmological constant. The field becomes dynamical at a critical redshift z_c as the Hubble friction decreases, eventually settling down around

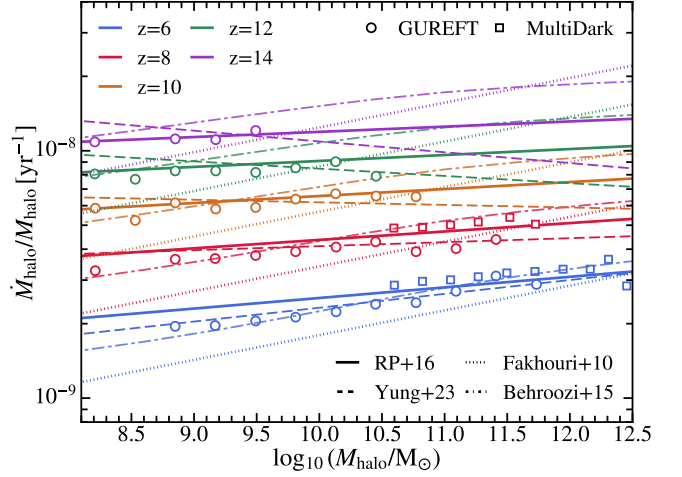


Figure 2. Halo specific accretion rate versus halo mass. We compare the halo accretion rates in [Fakhouri et al. \(2010\)](#) (adopted in [Shen et al. 2023](#)) with the fitting functions in [Behroozi & Silk \(2015\)](#), [Rodríguez-Puebla et al. \(2016b\)](#) (RP16), and [Yung et al. \(2024a\)](#). We also show the simulation results in GUREFT ([Yung et al. 2024a](#)) and MultiDark simulations ([Klypin et al. 2016](#)). [Behroozi & Silk \(2015\)](#) gives the mean accretion rate of M_{peak} and we correct it to the median value by assuming a 0.3 dex scatter in halo accretion rates (e.g. [Rodríguez-Puebla et al. 2016a](#); [Ren et al. 2019](#); [Mirocha et al. 2021](#)). It tends to overestimate the halo accretion rates in the massive end at $z \geq 10$. The [Fakhouri et al. \(2010\)](#) model underestimates the accretion rates in the low-mass end. The fitting in [Yung et al. \(2024a\)](#) is restricted to relatively low-mass haloes at high redshifts and it is unclear whether the fitted negative slope holds at $z \geq 10$. Therefore, we choose [Rodríguez-Puebla et al. \(2016b\)](#) as our new fiducial model.

the minimum of the potential and starting oscillation. The effective equation-of-state of the field afterward is $w_n \simeq (n-1)/(n+1)$. Here following [Smith et al. \(2022\)](#), we consider the $n = 3$ case, where the energy density of EDE dilutes faster than radiation. The existence of this additional pre-recombination energy density increases the Hubble parameter around the time of photon decoupling, and reduces the physical sound horizon if H_0 is fixed. Therefore, the inferred H_0 from the same sound horizon measurement on CMB will be increased with EDE. Since the energy density of the EDE field dilutes rapidly, it casts no direct impact on structure formation but its effects are indirectly imprinted through changes in cosmological parameters. We choose EDE and cosmological parameters as the best-fit values in [Smith et al. \(2022\)](#) constrained jointly by ACT, SPT, and Planck results. They are summarized in [Table 1](#) along with the best-fit parameters in the standard Λ CDM cosmology. The best-fit H_0 in the EDE cosmology is around $74 \text{ km s}^{-1} \text{Mpc}^{-1}$, in agreement with the local constraints.

2.1 Halo mass function

The halo mass function is constructed following Press-Schechter-like theories (e.g. [Press & Schechter 1974](#); [Bond et al. 1991](#); [Sheth et al. 2001](#)) as implemented in the HMF code ([Murray et al. 2013](#); [Murray 2014](#)). The transfer function is calculated using the Code for Anisotropies in the Microwave Background (CAMB; [Lewis et al. 2000](#); [Howlett et al. 2012](#)) and specifically the axion effective fluid

model¹ (Poulin et al. 2018) implemented there. Following Planck Collaboration et al. (2020), in both Λ CDM and EDE, we model free-streaming neutrinos as two massless and one massive species with $m_\nu = 0.06$ eV. The effective number of neutrino species N_{eff} is set to 3.046. We adopt a real-space top-hat filter function for the density field. The definition of halo mass follows the virial criterion in Bryan & Norman (1998). We adopt the halo mass function parametrization of Behroozi et al. (2013) to improve the accuracy at high redshift.

In Figure 1, we show the cumulative number density of haloes above a certain mass threshold as a function of redshift in the EDE and Λ CDM cosmology. The number densities of haloes are enhanced in the EDE model preferentially at high redshifts and at all mass scales because of the higher values of n_s , ω_{cdm} and σ_8 in EDE relative to the Planck Λ CDM cosmology (e.g. Klypin et al. 2021; Boylan-Kolchin 2023; Forconi et al. 2024). By $z = 0$, the halo mass functions are indistinguishable.

2.2 Halo accretion rate

We use the fitting function of halo accretion rate in Rodríguez-Puebla et al. (2016b)

$$\dot{M}_{\text{halo}} = C \left(\frac{M_{\text{halo}}}{10^{12} M_\odot / h} \right)^\gamma \frac{H(z)}{H_0}, \quad (1)$$

$$\gamma = 1.000 + 0.329 a - 0.206 a^2,$$

$$\log_{10} C = 2.730 - 1.828 a + 0.654 a^2,$$

where $a = 1/(1+z)$ is the scale factor. The \dot{M}_{halo} here is the median value at a given halo mass and is averaged over one dynamical time of the halo. This relation is calibrated on the Bolshoi-Planck and MultiDark-Planck cosmological simulations (Klypin et al. 2016). In Figure 2, we compare this fitting formula with relations found in other works (Fakhouri et al. 2010; Behroozi & Silk 2015; Yung et al. 2024b) and N-body simulation results (Klypin et al. 2016; Yung et al. 2024b). We find that the fitting function from Rodríguez-Puebla et al. (2016b) gives better agreement to simulations at high redshifts over a large dynamical range and therefore choose it as our fiducial model. We also note that the dependence of \dot{M}_{halo} on cosmology is fully absorbed in the $H(z)$ term and we expect it to hold in the EDE cosmology considered here as well.

2.3 Additional cosmological corrections

For predictions in the EDE model, the “interpreted” galaxy luminosities and number densities by an observer assuming Λ CDM should have additional corrections as

$$\Phi' = \Phi \times \frac{(dV/dz)_{\text{EDE}}}{(dV/dz)_{\Lambda\text{CDM}}},$$

$$M'_{\text{UV}} = M_{\text{UV}} + 2.5 \log_{10} \left((D_L^{\text{EDE}} / D_L^{\Lambda\text{CDM}})^2 \right), \quad (2)$$

where (dV/dz) and D_L are the differential comoving volume and luminosity distance at the redshift of interest. The galaxy stellar masses, luminosities, and number densities in the EDE cosmology will all be corrected values throughout this paper to form better comparisons with observational data.

¹ We have also experimented with the early quintessence model (Smith et al. 2020) implemented in CAMB and find $\lesssim 0.01$ dex differences between the halo mass function at $z = 10$ calculated using the transfer functions from the two EDE model implementations.

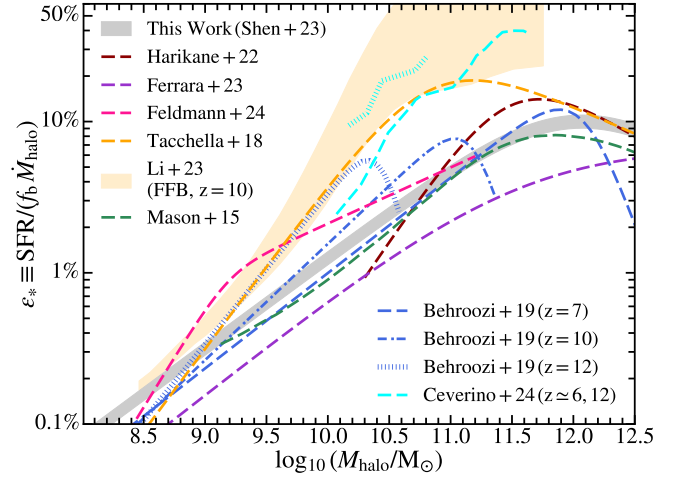


Figure 3. Star-formation efficiency (SFE) versus halo mass. We show the relation adopted in this work with the gray band, varying ϵ_* by $\pm 10\%$. We compare it with the SFE in other works (Mason et al. 2015; Tacchella et al. 2018; Behroozi et al. 2019; Harikane et al. 2022; Ferrara et al. 2023b; Li et al. 2023; Ceverino et al. 2024; Feldmann et al. 2024) as labelled. For the UNIVERSE MACHINE (Behroozi et al. 2019) and Ferrara et al. (2023b) predictions, we take their SFR- M_{halo} relations and convert it to SFE assuming our halo accretion rate model. For the FIREbox (Feldmann et al. 2024) predictions, we show the SFE based on the averaged SFR in the 100-Myr window. Li et al. (2023) adopted a modified version of Behroozi et al. (2019) with feedback-free starburst (FFB) in massive haloes. Results from the FirstLight simulations (Ceverino et al. 2024) show signatures of this regime at $z \approx 12$ (dotted cyan line). For the observational determination in Harikane et al. (2022), we scale it down to account for the different IMF choices.

3 EMPIRICAL GALAXY FORMATION MODEL

3.1 Star-formation and UV luminosity

In this section, we describe a **median** mapping between the observed galaxy UV luminosity and the host halo mass. All the empirical scaling relations we assume should be interpreted as median values. Since the mapping functions we use between \dot{M}_{halo} , star-formation rate (SFR), and UV luminosity are monotonic, the median operator is interchangeable with these mapping functions. This ensures that, for example, the mapped UV luminosity from the median \dot{M}_{halo} will be the same as the median UV luminosity mapped from the full \dot{M}_{halo} distribution.

We parameterize the SFR in dark matter haloes as $\text{SFR} = \epsilon_* f_b \dot{M}_{\text{halo}}$, where f_b is the universal baryon fraction and ϵ_* is the (halo-scale) SFE. Note that ϵ_* is a differential efficiency in our model while, in some work, the efficiency is defined as the cumulatively formed stellar mass relative to the available halo baryon reservoir. We adopt a redshift-independent double power-law function,

$$\epsilon_*(M_{\text{halo}}) = \frac{2 \epsilon_0}{(M_{\text{halo}}/M_0)^{-\alpha} + (M_{\text{halo}}/M_0)^\beta}, \quad (3)$$

where ϵ_0 is the peak SFE at the characteristic mass M_0 and α and β are the low-mass and high-mass end slopes, respectively. The functional form and the redshift-independent ansatz of Equation 3 have been used in previous empirical modeling works (e.g. Moster et al. 2010; Tacchella et al. 2018; Harikane et al. 2022; Shen et al. 2023). Following Shen et al. (2023), we adopt $\epsilon_0 = 0.1$, $M_0 = 10^{12} M_\odot$, $\alpha = 0.6$, $\beta = 0.5$ as our default values. The normalization and low-

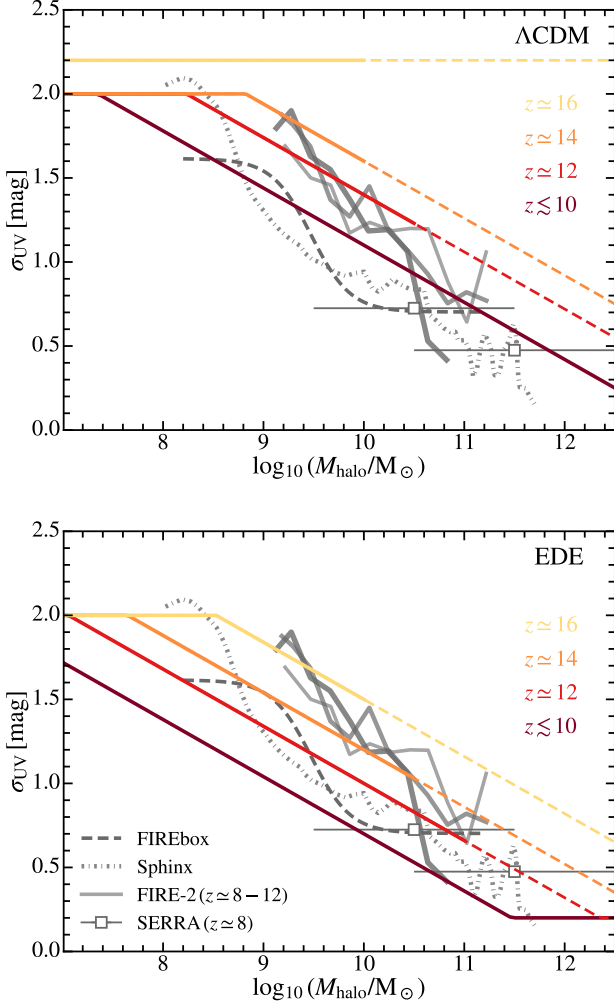


Figure 4. UV variability σ_{UV} versus M_{halo} . We show the parametric model adopted in this work, which roughly scales as $M_{\text{halo}}^{-1/3}$. Different values of the normalization factor A are preferred at different redshifts beyond ~ 10 . We compare it to the results from FIRE-2 zoom-in simulations (Sun et al. 2023a), the FIREbox simulation (Feldmann et al. 2024), the SPHINX simulations (Katz et al. 2023) as shown in Kravtsov & Belokurov (2024), and the SERRA simulations (Pallottini & Ferrara 2023). In both ΛCDM and EDE, a fixed $\sigma_{UV}-M_{\text{halo}}$ relation is capable of matching observational results at $z \lesssim 10$. However, at $z \gtrsim 12$, an enhancement of σ_{UV} is required and becomes prohibitively high at $z \approx 16$. In EDE, similar relative enhancement in σ_{UV} is inferred at $z \approx 12-14$ but the overall values of σ_{UV} agree reasonably with theoretical predictions. We note that the UVLFs at $z \gtrsim 10$ in the luminosity range probed by observations will not be sensitive to the variability in the massive end, which is indicated by the dashed lines.

mass slope were chosen to match the median SFR- M_{halo} relation at $z \approx 7$ from the UNIVERSE MACHINE (Behroozi et al. 2019). The parameter choices give good agreement with the observed UVLFs and UV luminosity densities at $z \lesssim 9$ as will later be demonstrated in Section 4.1.

This model is a basic representation of our knowledge about galaxy formation before the JWST era. In Figure 3, we compare our model of SFE versus halo mass with other choices in literature, including the observational constraints in Harikane et al. (2022) based on Halo Occupation Distribution, the UNIVERSE MACHINE predictions

at $z \approx 7-12$, the empirical models in Mason et al. (2015); Tacchella et al. (2018); Ferrara et al. (2023b), results from the FIREbox simulation (Feldmann et al. 2024), the feedback-free starburst (FFB) scenario at $z \approx 10$ (Li et al. 2023), and results from the FirstLight simulations (Ceverino et al. 2024, which aligns better with the FFB scenario at $z \gtrsim 10$). Our assumed $\epsilon_*-M_{\text{halo}}$ relation is a fair representation of the “median” of the models configured before the JWST era. However, we note the substantial uncertainties of the SFE (e.g. ϵ_* can vary between $\sim 1-10\%$ at $M_{\text{halo}} \sim 10^{10.5} M_{\odot}$ among models without entering the FFB regime) and the potential mild increase of SFE at higher redshifts found/assumed in some of these studies (e.g. Behroozi et al. 2019; Ceverino et al. 2024). Degeneracy in matching the UVLF does exist between the low-mass end SFE and other factors (e.g. Khimey et al. 2021; Shen et al. 2023; Muñoz et al. 2023), in particular UV variability, which will be discussed in the following sections.

We express the conversion between the SFR and the intrinsic UV-specific luminosity $L_{\nu}(\text{UV})$ (before dust attenuation) as

$$\text{SFR} [M_{\odot} \text{ yr}^{-1}] = \kappa_{UV} L_{\nu}(\text{UV}) [\text{erg s}^{-1} \text{ Hz}^{-1}] \quad (4)$$

with conversion factor $\kappa_{UV} = 0.72 \times 10^{-28}$ as in Madau & Dickinson (2014), where a Chabrier (2003) IMF is assumed and the (far-)UV wavelength is assumed to be 1500\AA .

We empirically model dust attenuation using a combination of the $A_{UV}-\beta$ (IRX- β) and $\beta-M_{UV}$ relations. The M_{UV} quoted here is the observed (dust-attenuated) UV magnitude. We adopt the relation $A_{UV} = 4.43 + 1.99\beta$ from Meurer et al. (1999). We adopt the $\beta-M_{UV}$ relation $\beta = -0.17 M_{UV} - 5.40$ from Cullen et al. (2023) at $8 \lesssim z \lesssim 10$ and the relation from Bouwens et al. (2014) at $z < 8$. Motivated by the extremely blue UV slopes of observed galaxies (e.g. Topping et al. 2022, 2024; Cullen et al. 2024), we assume no dust attenuation at $z > 10$, although uncertainties of dust attenuation in the observed luminous galaxies still exist (e.g. Bunker et al. 2023; Carniani et al. 2024; Castellano et al. 2024).

3.2 UV variability and its dependence on halo mass

Following Shen et al. (2023), we calculate galaxy rest-frame UVLF based on the underlying halo mass function as

$$\frac{dn}{dM_{UV}} = \frac{dn}{d \log_{10} M_{\text{halo}}} \left| \frac{d \log_{10} M_{\text{halo}}}{dM_{UV}} \right|, \quad (5)$$

and model the stochasticity of UV luminosity at fixed halo mass by convolving the UVLF with a Gaussian kernel of width σ_{UV} (in unit of AB magnitude). Effectively, this assumes that the observed UV luminosity has a log-normal distribution with the median value fixed by the scaling relations in Section 3.1. σ_{UV} effectively captures the scatter of galaxy UV luminosity due to the statistical scatter and time variability of star-formation rates (and dust attenuation) of individual sources.

Motivated by observational results and theoretical model predictions, we propose the following halo mass dependence of σ_{UV}

$$\sigma_{UV}(M_{\text{halo}}) = \text{MAX} [A(z) - B \log_{10}(M_{\text{halo}}/M_{\odot}), \sigma_{\text{min}}], \quad (6)$$

where we choose $B = 0.34$ which follows Gelli et al. (2024). This has been shown to agree well with the results of cosmological simulations (e.g. Sun et al. 2023a; Katz et al. 2023). $A(z)$ is a free parameter that encapsulates the potential redshift dependence of UV variability. $\sigma_{\text{min}} = 0.2$ mag is the floor of σ_{UV} we introduce better match the low-redshift UVLFs at the bright end (see Section 4.1, although similar agreement can be driven by tuning the massive-end slope β of the SFE model). In addition, we assume a maximum value

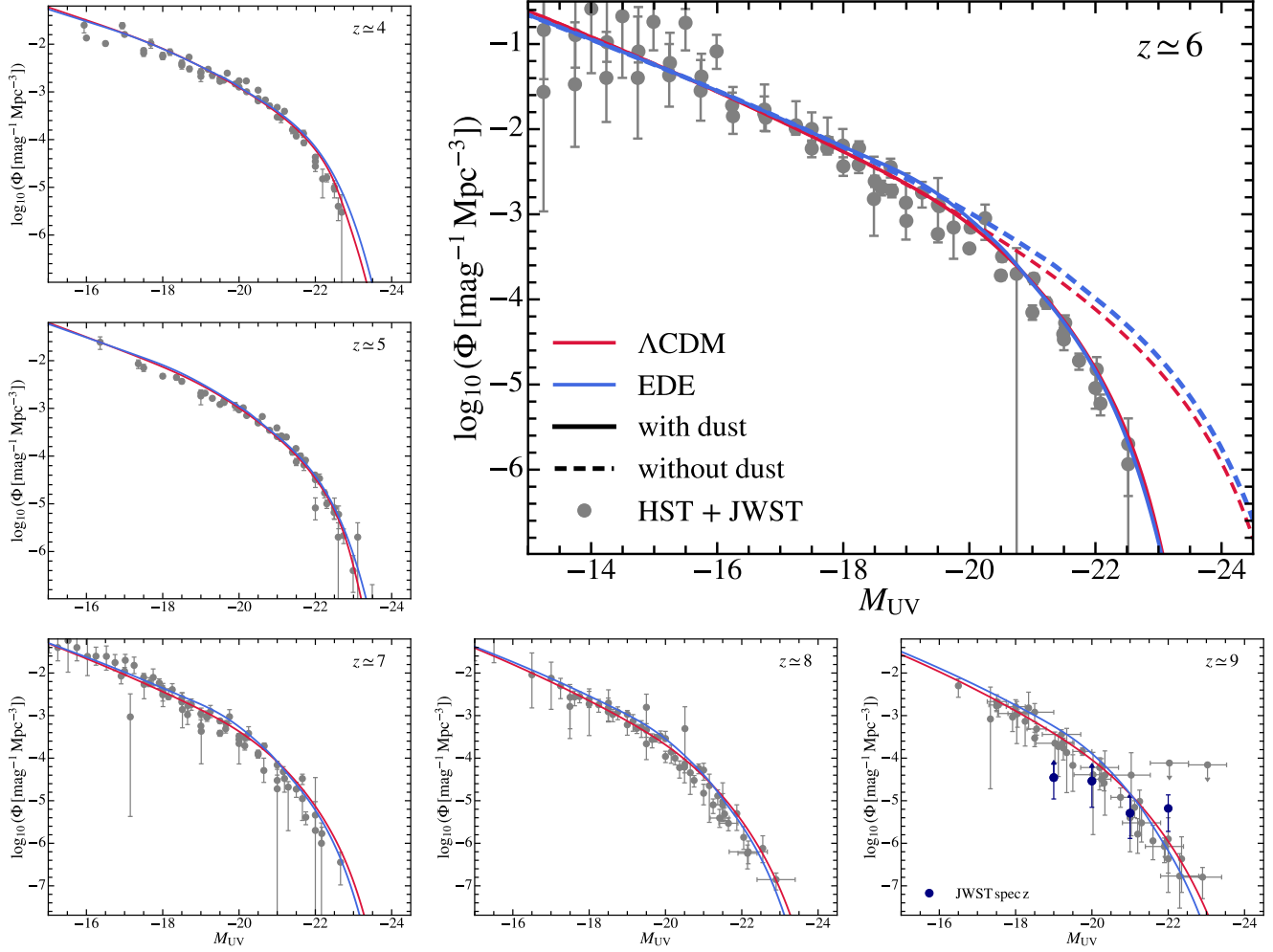


Figure 5. Galaxy rest-frame UVLFs at $4 \lesssim z \lesssim 9$ compared to observational constraints summarized in Section 4.1. The red (blue) curves show the predictions in Λ CDM (EDE) assuming a fixed A , which is the **only** parameter we tune here. In the top right panel, we highlight the $z \approx 6$ case and show the UVLFs with and without dust attenuation. This benchmark model shows remarkable agreement with observations across a wide range of redshifts and UV magnitudes. In particular, the agreement at the faint end is achieved by introducing the halo mass dependence of σ_{UV} .

of $\sigma_{\max} = 2$ mag in low-mass haloes. In Figure 4, we compare this UV variability model at different redshifts with results from various simulations² (Sun et al. 2023a; Pallottini & Ferrara 2023; Katz et al. 2023; Feldmann et al. 2024). As will be later introduced in Section 4.1 and 4.2, we identify the normalization term $A(z)$ to match the observed UVLFs at different redshifts. We will revisit this figure in Section 4.2 when we discuss the UVLFs at $z \gtrsim 10$.

In this paper, we have assumed a log-normal distribution of observed UV luminosity. However, in practice, a similar phenomenon can be driven by e.g. incorporating a fraction of starbursts with high SFEs. In Li et al. (2023), a feedback-free starburst (FFB) scenario with $\epsilon_*^{\max} = 0.2$ is suggested to explain observational results at $z \gtrsim 10$. Such a scenario can be roughly translated to a feedback-free phase ($\epsilon_* = 1$) with a duty cycle of 0.2 and otherwise the

normal phase ($\epsilon_* \sim 0.02$). The corresponding standard deviation in $\log_{10} \epsilon_*$ is around 0.68 dex (1.7 mag) above the FFB mass-scale $M_{\text{halo}} \sim 10^{10} M_{\odot}$ at $z \gtrsim 12$ (Dekel et al. 2023).

4 RESULTS

4.1 Benchmark the model at $4 \lesssim z \lesssim 9$

As the first step, we calibrate our model based on the observational constraints of UVLFs at $4 \lesssim z \lesssim 9$. In this paper, we include the HST observations compiled in Vogelsberger et al. (2020) and those from McLeod et al. (2016); Oesch et al. (2018); Morishita et al. (2018); Stefanon et al. (2019); Bowler et al. (2020); Bouwens et al. (2021). For JWST constraints, we include constraints based on photometrically selected galaxies from Castellano et al. (2022); Finkelstein et al. (2022); Naidu et al. (2022b); Adams et al. (2023a); Bouwens et al. (2023b,a); Donnan et al. (2023); Harikane et al. (2023); Leethochawalit et al. (2023); Morishita & Stiavelli (2023);

² We adopt a crude estimate of the host halo mass of the two galaxies presented in Pallottini & Ferrara (2023) based on the stellar-to-halo mass relation in Behroozi et al. (2019).

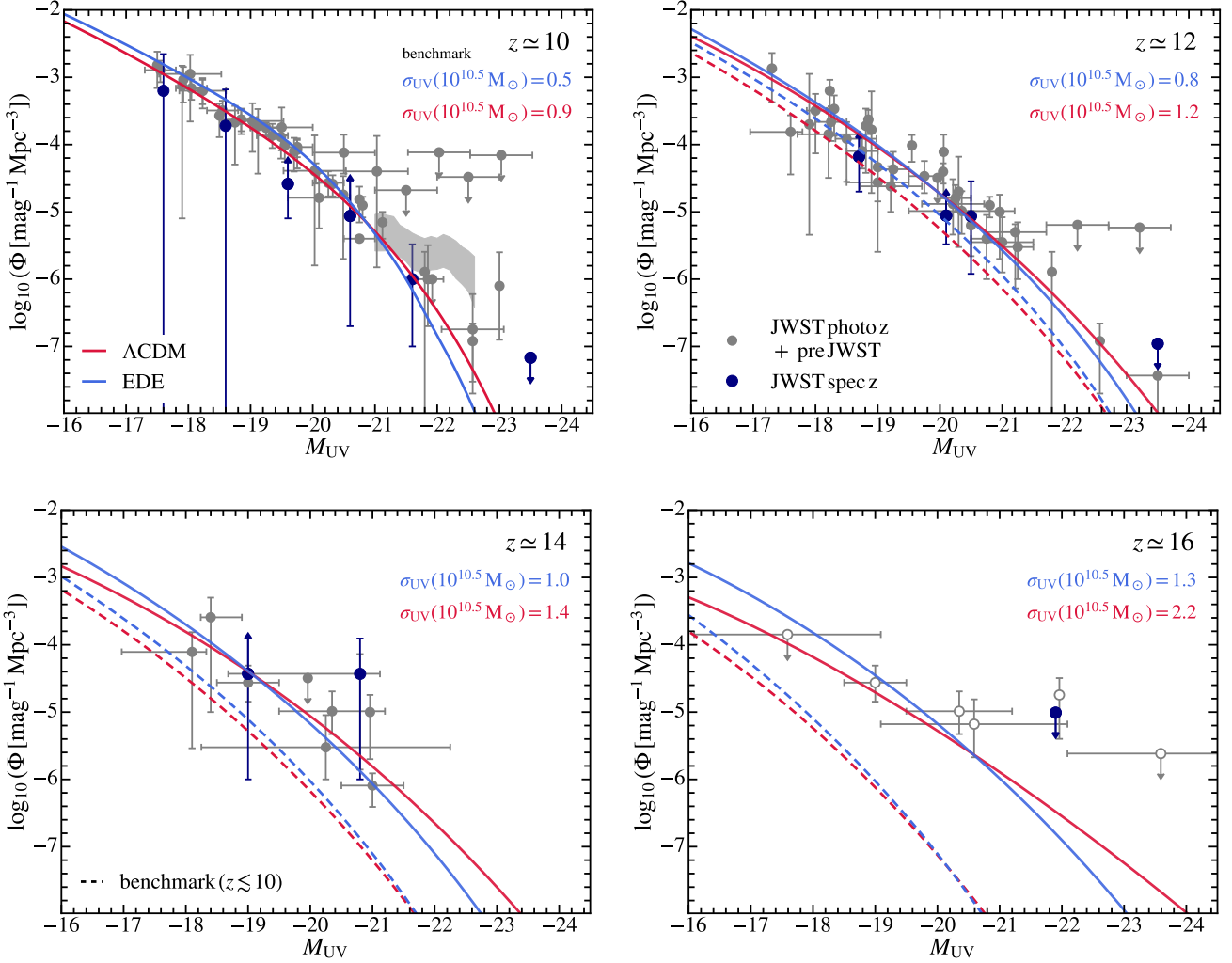


Figure 6. Galaxy rest-frame UVLFs at $z \geq 10$ in ΛCDM (red) and EDE (blue), compared to observational constraints (the solid points). The observational measurements at $z \approx 16$ are purely based on photometrically selected galaxies and are shown with open markers. The solid lines show the predictions with the tuning of the normalization of the $\sigma_{\text{UV}}-M_{\text{halo}}$ relation, $A(z)$, although one could also tune the SFE to achieve a similar level of agreement. The suggested values of σ_{UV} at $10^{10.5} M_{\odot}$ are labelled in each panel. We compare them to the observational constraints summarized in Section 4.1. The benchmark model in EDE agrees with the spectroscopic constraints at $z \approx 12$. Although moderately higher σ_{UV} is suggested to match the photometric constraints at $z \approx 12$ and 14, the σ_{UV} values are about 0.4 mag smaller than in the ΛCDM case. Moreover, at $z \approx 16$, the extreme observational constraints can be reconciled with σ_{UV} at $10^{10.5} M_{\odot} \approx 1.3$ mag in EDE while an unphysically high $\sigma_{\text{UV}} \approx 2.2$ mag is required in ΛCDM .

Pérez-González et al. (2023); Robertson et al. (2023b); McLeod et al. (2024); Donnan et al. (2024); Casey et al. (2024). Furthermore, we include constraints based only on spectroscopically-confirmed galaxies (Harikane et al. 2024b,a, see the references therein).

We adopt the redshift-independent but halo mass-dependent SFE described in Section 3.1 and only allow the normalization term $A(z)$ of UV variability to vary (as the variability is less constrained compared to SFE in literature). Notably, we find that a redshift-independent choice of $A = 4.5$ ($A = 4.1$) in ΛCDM (EDE) leads to UVLFs that are consistent remarkably with observations across the entire redshift range. In Figure 5, we show the results of the calibrated models compared to the observed UVLF at $4 \lesssim z \lesssim 9$. Compared to Shen et al. (2023), the halo mass dependence of σ_{UV} helps us realize a better agreement with the faint-end of UVLF across redshifts. Similar results have recently been demonstrated in Gelli et al. (2024).

These preferred $\sigma_{\text{UV}}(M_{\text{halo}})$ relations at $z \lesssim 10$ are also shown in Figure 4. This calibrated model will be referred to as the benchmark model in the following analysis.

4.2 UVLF at $z \geq 10$

We now explore the model variations necessary at $z \geq 10$ to reconcile observations with theoretical model predictions in ΛCDM versus EDE. Due to the degeneracy between the SFE in the low-mass end and UV variability on UVLF predictions, variation in either direction has the potential to resolve the UVLF tension (see also Muñoz et al. 2023). In this Section, we focus on varying the UV variability by adjusting the normalization $A(z)$ and defer the discussion on the alternative SFE solution to Figure 7. Since the slope of the $\sigma_{\text{UV}}-M_{\text{halo}}$ relation is fixed, we will denote the change to $A(z)$ with σ_{UV}

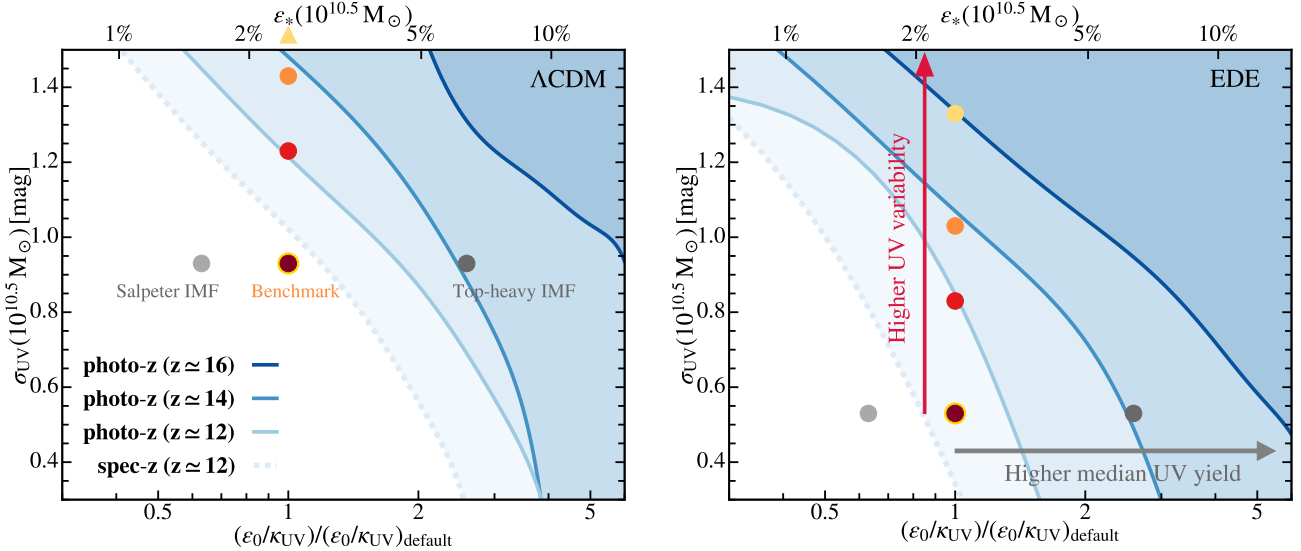


Figure 7. Parameter space of UV variability, characterized by $\sigma_{\text{UV}}(10^{10.5} M_{\odot})$, versus median UV radiation yield, represented by $\epsilon_0/\kappa_{\text{UV}}$. If the change in median UV radiation yield is purely driven by the change in SFE, the corresponding ϵ_* at $M_{\text{halo}} = 10^{10.5} M_{\odot}$ is labelled. The axis ranges are chosen to roughly cover the ϵ_* values assumed in different studies (Figure 3) and the σ_{UV} values found in numeric simulations (Figure 4). The shaded regions show the regions of parameter space consistent with the JWST results mapped by our empirical model. The deeper the color, the more challenging it is to reconcile the constraints. The left (right) panel shows the results in the ΛCDM (EDE) model. The fiducial model assumes [Chabrier \(2003\)](#) IMF. In the horizontal direction, we show the changes in median UV radiation yield for the [Salpeter \(1955\)](#) IMF and a top-heavy IMF in [Inayoshi et al. \(2022\)](#) with gray circles. In the vertical direction, we show the changes in UV variability required to match different levels of observational constraints with colored circles that match values shown in Figure 4 and Figure 6.

at a characteristic halo mass $10^{10.5} M_{\odot}$. In the benchmark model, $\sigma_{\text{UV}}(10^{10.5} M_{\odot}) = 0.9$ and 0.5 mag in the ΛCDM and EDE cosmologies, respectively.

Figure 6 shows the UVLFs obtained from our model at $z \gtrsim 10$. At $z \approx 10$, predictions from the benchmark models in both ΛCDM and EDE continue to match observations without further tuning. At $z \approx 12$, to match the spectroscopic constraints, a small $\lesssim 0.1$ mag enhancement of UV variability is sufficient for the ΛCDM . Meanwhile, the benchmark model in EDE works without any change to $\sigma_{\text{UV}}(10^{10.5} M_{\odot})$. Similar findings have been discussed in [Gelli et al. \(2024\)](#), where the halo mass dependence of UV variability can reduce the need for model variations at $z \approx 12$. To match the photometric constraints at the same redshift, $\sigma_{\text{UV}}(10^{10.5} M_{\odot})$ needs to be enhanced to ≈ 1.2 (0.8) mag to match observational constraints in ΛCDM (EDE). However, the discrepancies between observations and the predictions of benchmark models are relatively small ($\lesssim 0.3$ dex) and fall within the uncertainties from halo mass function calculations (e.g. [Yung et al. 2024a](#)) and cosmic variances (e.g. [Yung et al. 2024b](#); [Kragh Jespersen et al. 2024](#)).

At $z \approx 14$, $\sigma_{\text{UV}}(10^{10.5} M_{\odot}) \approx 1.4$ (1.0) mag is preferred in ΛCDM (EDE), although the benchmark model predictions are still within the $1\text{-}\sigma$ error bar of observational constraints from e.g. [Donnan et al. \(2024\)](#). Two galaxy candidates at $z \approx 14$ have recently been spectroscopically confirmed ([Carniani et al. 2024](#)) and show signatures of a strong recent starburst in MIRI band ([Helton et al. 2024](#)). At $z \approx 16$, in ΛCDM , we find that a simple adjustment of $A(z)$ is no longer feasible to reconcile observations and we have to increase σ_{UV} to ≈ 2.2 mag, ignoring the σ_{max} we imposed. The model becomes equivalent to the constant σ_{UV} model explored in

[Shen et al. \(2023\)](#)³. We note that the UV variability in the massive end will not impact the UVLF in the observed range⁴, as indicated by the dashed lines in Figure 4. Nevertheless, such a high σ_{UV} exceeds the maximum value found in cosmological hydrodynamical simulations (see Figure 4). As discussed in [Kravtsov & Belokurov \(2024\)](#), it could lead to instantaneous SFE exceeding unity when modelling the bursty star-formation history of galaxies. On the contrary, in the EDE model, $\sigma_{\text{UV}}(10^{10.5} M_{\odot})$ only needs to be enhanced moderately to ≈ 1.3 mag to reconcile observations with theoretical model predictions. This significantly eases the level of model adjustment to account for these extreme constraints. We summarize these suggested $\sigma_{\text{UV}}(M_{\text{halo}})$ at different redshifts in Figure 4. In ΛCDM , the implied σ_{UV} values at $z \approx 14$ are close to the maximum value found in existing cosmological hydrodynamical simulations and the σ_{UV} values at $z \approx 16$ exceed substantially this maximum. However, in the EDE cosmology, the suggested σ_{UV} values are safely among the scatters of simulation results.

4.3 Explore the model parameter space

To illustrate various model variations to reconcile JWST results with theoretical models, Figure 7 examines the parameter space of UV variability and the median UV radiation yield in the ΛCDM and EDE cosmology. For results based on JWST spectroscopy, we adopt the lower limit estimated in [Harikane et al. \(2024b,a\)](#) at $z \approx 12$. For photometric constraints, we consider the model to be

³ The small difference in σ_{UV} inferred is mainly caused by changing the IMF to [Chabrier \(2003\)](#) in this work from [Salpeter \(1955\)](#) in [Shen et al. \(2023\)](#).

⁴ We obtain this mass range by manually setting UV variability above some mass threshold to the benchmark model values and check if the resulting UVLF is still consistent with observations.

acceptable when $\log_{10} \Phi(M_{\text{UV}} = -20) > -4.8$ at $z \approx 12$, and $\log_{10} \Phi(M_{\text{UV}} = -19) > -4.4$ and -4.5 at $z = 14$ and 16. These are fairly rough estimates (i.e. without a quantitative measure of fitting residuals), but we have explicitly examined the UVLF predictions around these threshold values and find that they capture the goodness of fit reasonably well. We scan the parameter space by modifying UV variability ($A(z)$ or equivalently $\sigma_{\text{UV}}(10^{10.5} M_{\odot})$) and the normalization of the SFE in our model, and identify the regime where theoretically predicted UV bright galaxy abundance exceeds the observed values. We also show the impact of IMF variations as in Shen et al. (2023), where a Salpeter IMF leads to about 60% increase in κ_{UV} (Madau & Dickinson 2014) and an extremely top-heavy IMF (e.g. Inayoshi et al. 2022) leads to κ_{UV} dropping by 55%.

In ΛCDM , the benchmark model is only slightly off from the spectroscopic constraints of JWST. The required model variations are much smaller compared to Shen et al. (2023). This is mainly due to the change to Chabrier (2003) IMF and the indirect enhancement of UV variabilities from the halo mass dependence. Galaxies with the same UV luminosity are hosted by lower mass haloes at higher redshifts and thus exhibit higher σ_{UV} even in the absence of redshift-dependence of σ_{UV} . In the EDE cosmology, the out-of-the-box prediction at $z \approx 12$ is fully consistent with the spectroscopic constraints. As also demonstrated in Figure 6, the UV variability needs to be increased to match photometric constraints at $z \approx 12$ and 14. The required values of $\sigma_{\text{UV}}(10^{10.5} M_{\odot})$ in EDE are significantly smaller than those in ΛCDM and are more consistent with predictions from numeric simulations. Alternatively, one could also reconcile the observations by boosting the SFE or incorporating a top-heavy IMF to increase the light-to-mass ratio. Along this orthogonal direction, agreement with observations is also easier to achieve in the EDE cosmology compared to the ΛCDM case. A small factor of ~ 1.5 (2.5) boost in UV photon yield is necessary for the $z \approx 12$ (14) photometric constraints, which corresponds to $\epsilon_*(10^{10.5} M_{\odot}) \approx 3\%$ (6%). These are feasible given the uncertainties of SFE in low-mass haloes as shown in Figure 3.

Qualitative differences show up when confronting the $z \approx 16$ constraints. In ΛCDM , an extremely high, constant $\sigma_{\text{UV}} \approx 2.2$ mag is required, which would imply a strong non-linear transition of UV variability at $z \gtrsim 14$. In the EDE cosmology, it becomes feasible with a suggested $\sigma_{\text{UV}}(10^{10.5} M_{\odot}) \approx 1.3$ mag. One could also achieve this by boosting the SFE by a factor of ~ 5 and the implied ϵ_* at $\sim 10^{10.5} M_{\odot}$ will be $\sim 10\%$, which is below the maximum value found in literature and could be easily reached in the FFB scenario (Li et al. 2023). The introduction of EDE eases the level of tuning to the galaxy formation model to reconcile these extreme JWST results. However, we are cautious in making strong conclusions about ΛCDM based on the comparison at this redshift, since the constraints here are largely based on a handful of photometrically-selected galaxies (e.g. Bouwens et al. 2023b; Harikane et al. 2023) and remain uncertain.

4.4 Host haloes of UV-bright galaxies at cosmic dawn

In Figure 8, we show the UVLFs at $z \approx 14$ in four different scenarios that could equally well match observational constraints. This includes the model with constant σ_{UV} as explored in Shen et al. (2023), the approach of boosting the SFE by three times with respect to the benchmark model at low redshifts (see similar values found in e.g. Yung et al. 2024b), and the approach of adjusting the normalizations of $\sigma_{\text{UV}}(M_{\text{halo}})$ in the ΛCDM and EDE cosmologies as discussed above. However, due to different levels of σ_{UV} adopted, the host halo mass of observed UV-bright galaxies can be rather different in these

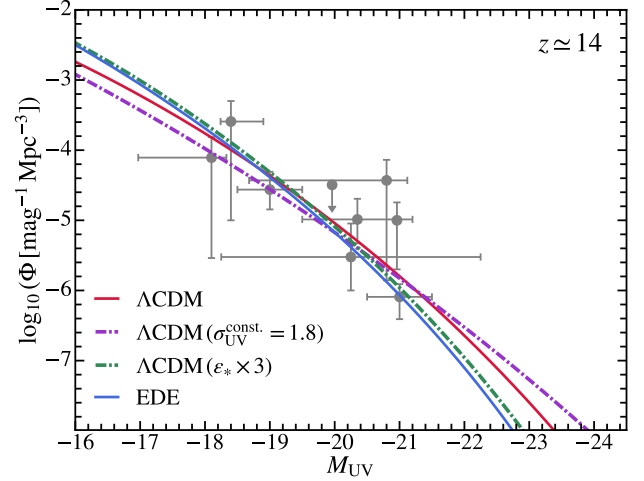


Figure 8. Galaxy UVLF at $z \approx 14$ in the following four scenarios: (1) the constant UV variability model considered in Shen et al. (2023); (2) boosting the SFE by a factor of three while assuming the benchmark $\sigma_{\text{UV}}(M_{\text{halo}})$ in ΛCDM ; (3) adopt appropriate modifications to the normalization of $\sigma_{\text{UV}}(M_{\text{halo}})$ in ΛCDM and (4) EDE, respectively. The observed UVLF at $z \approx 14$ are equally well explained by these adjustments to the galaxy formation model.

scenarios. In the top panel of Figure 9, we show the median host halo mass of galaxies at a given M_{UV} at $z \approx 14$. Assuming only varying UV variability, the typical halo mass of observed galaxies in ΛCDM is around $10^9 M_{\odot}$ at $z \approx 14$, the mass scale of current-day ultra-faint dwarfs. The descendants of these haloes will end up with $\sim 10^{13} - 10^{14} M_{\odot}$ when evolving to $z = 0$ (e.g. Lu et al. 2024). However, in the EDE cosmology, due to the much smaller σ_{UV} required, the host haloes are about 0.5 - 1 dex heavier than in ΛCDM . It is even more of the case if one attempts to solve the tension by only adjusting SFE. We find that the host halo mass in this scenario will be around $10^{10.5} M_{\odot}$.

The different host halo masses can lead to different clustering powers of observed UV-bright galaxies. Following e.g. Muñoz et al. (2023); Gelli et al. (2024), we calculate the number density-normalized, effective bias of galaxies at fixed UV luminosity as

$$b_{\text{eff}}(M_{\text{UV}}) = \frac{1}{\Phi(M_{\text{UV}})} \int dM_{\text{halo}} \frac{dn}{dM_{\text{halo}}} b(M_{\text{halo}}) P(M_{\text{halo}}|M_{\text{UV}}), \quad (7)$$

where $\Phi(M_{\text{UV}})$ is the UVLF, $P(M_{\text{halo}}|M_{\text{UV}})$ is the conditional probability distribution of halo mass at a given M_{UV} , $b(M_{\text{halo}})$ is the halo bias calculated using the Tinker et al. (2010) model as implemented in the COLUSSUS package (Diemer 2018). In the bottom row of Figure 9, we show b_{eff} versus the observed M_{UV} . Models with higher UV variability predict lower b_{eff} in general. The differences show up primarily at the bright end. It is worth noting that even assuming the same galaxy-halo mapping, the bias in the EDE cosmology will still be smaller than that in ΛCDM due to the larger H_0 value. This makes the galaxy bias difference between EDE and ΛCDM smaller than naively inferred from the $M_{\text{UV}}-M_{\text{halo}}$ relation. Measurements of the environment of these UV-bright galaxies may help distinguish these degenerate scenarios. Potential avenues include measurements of reionization bubble sizes (e.g. Hsiao et al. 2023; Umeda et al. 2023; Nadler et al. 2023, and see a recent theoretical study by Neyer

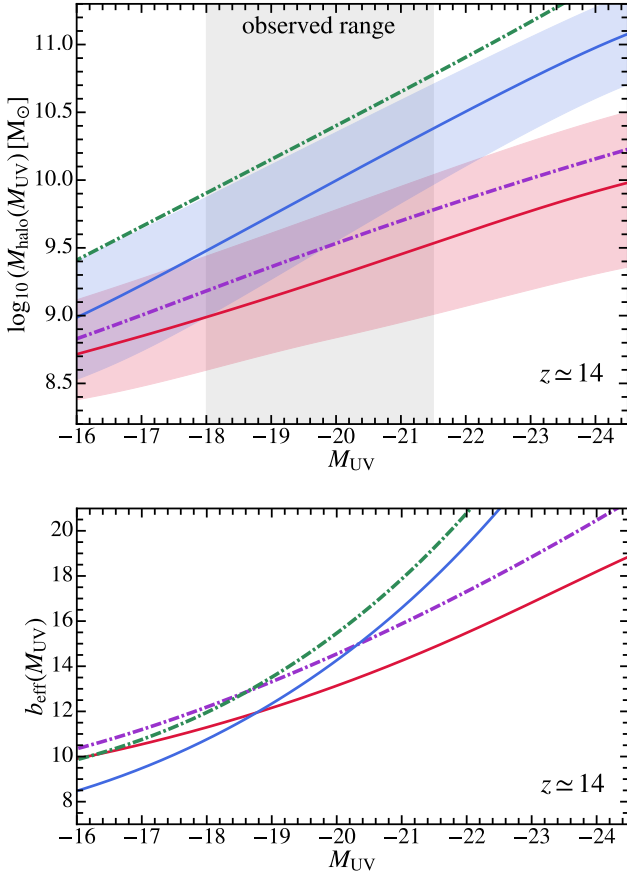


Figure 9. *Top:* Median halo mass at a given observed UV magnitude, M_{UV} , at $z \approx 14$. We consider the same four scenarios as shown in Figure 8 and adopt the same labelling. The gray-shaded region shows the typical luminosity range of observed galaxies at this redshift. *Bottom:* Effective bias of galaxies as a function of M_{UV} . Due to the lower host halo mass in model variations with larger UV variability, the bias of bright galaxies is significantly reduced.

et al. 2024), simple neighbor searches (e.g. Tacchella et al. 2023b), and future galaxy clustering measurements with JWST and Roman.

4.5 Implications for the overly-massive galaxies

Another natural consequence of enhanced halo abundance in EDE is the increased number density of massive galaxies. Early JWST observations have revealed several overly massive galaxy candidates exceeding expectations in the standard galaxy formation model given the field of view of observations (e.g. Labbé et al. 2023; Xiao et al. 2023; Casey et al. 2024). Some even require converting all the baryons in the Universe to stars to produce, thus challenging the Λ CDM model (e.g. Boylan-Kolchin 2023; Lovell et al. 2023). While the stellar mass estimates of these galaxies are uncertain (e.g. Endsley et al. 2023b; Chworowsky et al. 2023; Narayanan et al. 2024; Wang et al. 2024b) and even their “galaxy or AGN” identification is subject to debates (e.g. Kocevski et al. 2023; Desprez et al. 2024; Wang et al. 2024b), our exploration here delves into how this tension would manifest within the framework of EDE cosmology.

We derive the stellar-to-halo mass relation of galaxies by integrat-

ing the SFE in Equation 3

$$M_*(M_{\text{halo}}) = (1 - R) \left[\epsilon_*(M_{\text{min}}) M_{\text{min}} + \int_{M_{\text{min}}}^{M_{\text{halo}}} dM'_{\text{halo}} f_b \epsilon_*(M'_{\text{halo}}) \mathcal{F}(\sigma_{\text{sfr}}) \right], \quad (8)$$

where $M_{\text{min}} = 10^8 M_{\odot}$ is the minimum halo mass we start from (the SFE below which is assumed to be a constant) which does not affect our result, R is the mass return fraction of stars taken to be 0.1 for the young and low-metallicity stellar populations at high redshifts (e.g. Hopkins et al. 2018, 2023; Feldmann et al. 2024), $\mathcal{F}(\sigma_{\text{sfr}})$ is the factor considering the difference between mean SFR and median SFR with the logarithm scatter σ_{sfr} in unit of dex

$$\mathcal{F}(\sigma_{\text{sfr}}) = \exp\left(\ln 10 \sigma_{\text{sfr}}^2 / 2\right). \quad (9)$$

If the UV variability is dominated by the burstiness of star-formation, we have $\sigma_{\text{sfr}} = \sigma_{UV}/2.5$. We include this factor when calculating the integrated stellar mass density, but remove it when calculating e.g. median stellar mass given halo mass. We have verified that this approach gives consistent stellar-to-halo mass ratios with abundance-matching results (e.g. Behroozi et al. 2013, 2019; Rodríguez-Puebla et al. 2017). We obtain the cumulative cosmic stellar mass density above M_* as

$$\rho_*(> M_*) = \int_{M_{\text{halo}}(M_*)}^{\infty} dM'_{\text{halo}} \frac{dn}{dM'_{\text{halo}}} M_*(M'_{\text{halo}}), \quad (10)$$

where we effectively assume the scatter in galaxy stellar mass is negligible after aggregating many cycles of stochastic star-formation. The maximum stellar mass density allowed by cosmology is

$$\rho_*^{\text{max}}(> M_*) = \int_{M_{\text{halo}}(M_*)}^{\infty} dM'_{\text{halo}} \frac{dn}{dM'_{\text{halo}}} f_b M'_{\text{halo}}. \quad (11)$$

In Figure 10, we compare the stellar mass density in Λ CDM and EDE with observational constraints from JWST. We show the model predictions at $z \approx 8, 9, \text{ and } 12$, which corresponds to the constraints from CEERS (Labbé et al. 2023), COSMOS-Web (Casey et al. 2024), RUBIES (Wang et al. 2024a), and Akins et al. (2023). For reference, we also show estimates by integrating the Schechter function fits of stellar mass functions from Stefanon et al. (2021); Weibel et al. (2024) and Harvey et al. (2024). A notable tension emerges with the Labbé et al. (2023) results surpassing the maximum achievable stellar mass density in the Λ CDM framework. However, EDE exhibits no such challenge, with all data points comfortably below the maximum threshold at the $1\text{-}\sigma$ level. It is feasible to produce these massive galaxies with a physically realistic SFE. The stellar mass density produced by our fiducial star-formation model (with $A(z)$ chosen to match the UVLF at the corresponding redshift) in EDE is marginally consistent with findings from Wang et al. (2024a) and Desprez et al. (2024) at $z \approx 8$ (who revisited the CEERS sample and tested removing the single most massive outlier), and the Cosmos-Web results at $z \sim 10$ (Casey et al. 2024). However, discrepancies persist at $z \approx 12$. We explore two potential model variations, increasing $A(z)$ such that $\sigma_{UV}(10^{10.5}) \approx 1.3$ mag or increasing the SFE by five times. As shown in Figure 7, these two can make the UVLF at $z \approx 16$ consistent with observations. Since the impact of UV variability on ρ_* is primarily through $\mathcal{F}(\sigma_{\text{sfr}})$, it is very hard to reconcile observations purely on the UV variability direction. Alternatively, a heightened SFE emerges as a potential solution for reconciling the model with observational discrepancies in this context, as it not only increases the M_* at a given M_{halo} but also lowers the integration range in Equation 10.

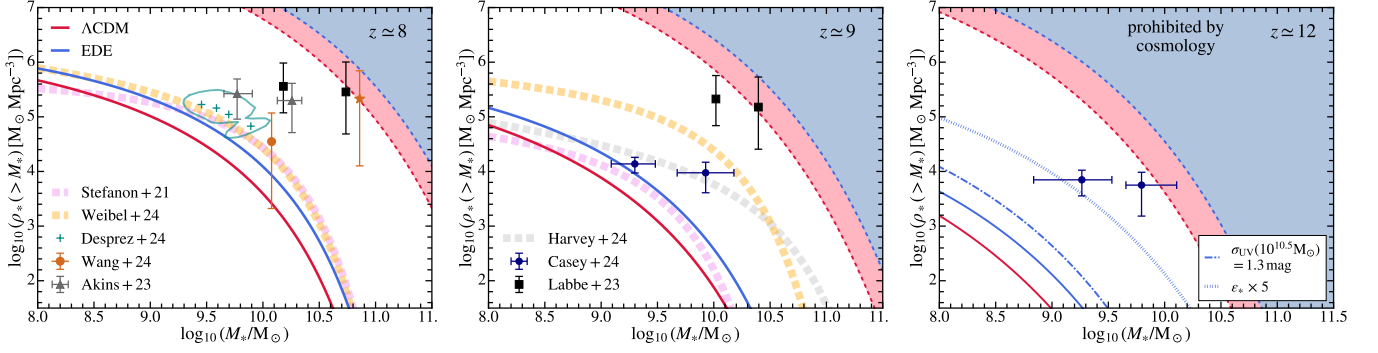


Figure 10. Cosmic stellar mass density for galaxies with stellar mass above M_* at $z \approx 8, 9,$ and 12 . The dashed lines show the upper limit derived by converting all the baryons in the Universe to stars in the assumed cosmology. The solid lines show predictions from our benchmark model at $z \approx 8, 9,$ and the slightly tuned model at $z \approx 12$ which match the UVLF constraints in Figure 6. The dotted and dotted-dashed lines show two alternative scenarios in EDE when (1) $\sigma_{\text{UV}}(10^{10.5} M_\odot)$ is further increased to 1.3 mag (the value needed for the $z \approx 16$ UVLF constraints) or (2) SFE is enhanced by a factor of five. We compare them to the observational constraints from JWST reported in [Labbé et al. \(2023\)](#); [Akins et al. \(2023\)](#); [Casey et al. \(2024\)](#), and [Wang et al. \(2024a\)](#) (“medium” estimate as the circle, “maximum” as the star). [Desprez et al. \(2024\)](#) revisited the CEERS sample used in [Labbé et al. \(2023\)](#) and derived alternative constraints when the single most massive outlier was removed. We also show estimates by integrating the Schechter function fits of stellar mass functions from [Stefanon et al. \(2021\)](#); [Weibel et al. \(2024\)](#); [Harvey et al. \(2024\)](#). IMF-related corrections on stellar masses are made for all these data. The most extreme observational constraints from JWST, which are in conflict with ΛCDM , can be safely accommodated in the EDE cosmology. The benchmark model predictions at $z \approx 8$ and 9 marginally agree with some less stringent observational constraints. At $z \approx 12$, a boosted SFE can better explain the large cosmic stellar mass densities compared to enhanced UV variabilities.

Many massive galaxy candidates mentioned above belong to the population of compact and extremely red galaxies found by JWST at $z \gtrsim 4$, known as the Little Red Dots (LRDs; e.g. [Matthee et al. 2024](#); [Kocevski et al. 2024](#); [Kokorev et al. 2024](#)). Similar to what we discussed above, if these LRDs are all interpreted as massive galaxies, the implied stellar mass densities exceed the maximum value allowed by the total baryon content in the Universe (e.g. [Akins et al. 2024](#)). Since many of them show broad Balmer emission lines as a signature of AGN, a more plausible interpretation of these LRDs is heavily obscured AGN. However, in this scenario, their number densities are still much larger than extrapolated from pre-JWST observations in UV and X-ray (e.g. [Aird et al. 2015](#); [Kulkarni et al. 2019](#); [Shen et al. 2020](#); [Niida et al. 2020](#)) and some theoretical model predictions after considering their heavy obscuration. As we shown in Figure 1, the increase in halo number density at $z \approx 6 - 8$ is about 0.3 – 0.5 dex in EDE compared to the standard ΛCDM cosmology and this level of difference could alleviate these puzzles of the general LRD population as well.

5 DISCUSSION AND CONCLUSIONS

We investigate the UVLF of galaxies at $4 \lesssim z \lesssim 16$ in the standard ΛCDM and EDE cosmologies. The specific EDE model we consider has the implication of solving the Hubble tension by reducing the sound horizon at the CMB epoch. As a byproduct of this, the cosmological parameters are changed in EDE such that the abundance of dark matter haloes is systematically enhanced compared to ΛCDM at high redshift ($z \gtrsim 8$). We describe an empirical galaxy formation model incorporating SFE and UV variability of galaxies that depends on host halo mass. Our benchmark model, with no redshift dependence of SFE or UV variability, can predict UVLF that is consistent with observations at $4 \lesssim z \lesssim 10$. We find that compared to the model with constant UV variability, the halo mass dependence significantly improves the agreement with the observed UVLFs in the faint end.

At higher redshifts ($z \gtrsim 10$), we examined the necessary model

variations to reconcile theoretical predictions with observations. We take the approach of adjusting the normalization of $\sigma_{\text{UV}}-M_{\text{halo}}$ relation and alternatively one can also achieve this by adjusting the SFE. Although a moderate level of enhancement in UV variability is still suggested in EDE, the σ_{UV} values are consistent with the predictions from hydrodynamical simulations. On the contrary, in ΛCDM , substantially higher σ_{UV} values are suggested and, in particular at $z \approx 16$, unphysically high σ_{UV} is required. This suggests that EDE may offer a more feasible framework for understanding galaxy formation and evolution during cosmic dawn.

Furthermore, the enhanced halo abundance in EDE completely resolves the tension between a handful of potentially ultra-massive galaxies and the maximum stellar mass density allowed by cosmology. In the EDE cosmology, the benchmark galaxy formation model is quantitatively consistent with some stringent observational constraints without fine-tuning.

Due to different levels of σ_{UV} inferred, galaxies in the EDE cosmology are hosted by more massive haloes. This difference in host halo mass is reflected in the effective bias of galaxies, which varies in order of magnitudes between models with enhanced SFE, constant σ_{UV} , halo mass-dependent σ_{UV} in different cosmologies. Future observations may be able to distinguish these somewhat degenerated scenarios through clustering measurements. As shown in Figure 3 and Figure 4, cosmological simulations of galaxy formation at high redshifts are still far from reaching converged results in terms of SFE and UV variability. The major uncertainties originate from the explicit modelling of star-formation and multiple channels of stellar feedback in resolved ISM (e.g. [Iyer et al. 2020](#); [Zhang et al. 2024](#)), potentially entangled with AGN feedback, variable IMF, etc. JWST observations offer new opportunities to constrain this class of galaxy formation models in simulations, such as emission line measurements (e.g. [Endsley et al. 2023a](#); [Sun et al. 2023b](#); [Boyett et al. 2024](#); [Helton et al. 2024](#)), size and morphological constraints (e.g. [Baggen et al. 2023](#); [Robertson et al. 2023a](#); [Morishita et al. 2024](#); [de Graaff et al. 2024b](#); [Shen et al. 2024](#); [Fujimoto et al. 2024](#)), as well as chem-

ical enrichment patterns (e.g. [Bunker et al. 2023](#); [Curti et al. 2023](#); [Cameron et al. 2023](#)). Narrowing down the uncertainties in SFE and variability and their redshift evolution can help disentangle the solutions through baryonic physics versus cosmology. Meanwhile, direct constraints on EDE and all “early” solutions to the Hubble tension can be obtained by independent measurements of the age of the Universe from e.g. globular clusters, white dwarfs, and metal-poor stars in the local Universe (e.g. [Winget et al. 1987](#); [Cowan et al. 1991](#); [Chaboyer 1995](#); [Vandenberg et al. 1996](#); [Verde et al. 2019](#)), but systematic uncertainties remain large (e.g. [Boylan-Kolchin & Weisz 2021](#); [Ying et al. 2023](#)).

Our findings highlight the potential of using observed galaxy abundance at cosmic dawn to constrain cosmological models. Specifically, the EDE model shows promise in providing a unified solution to the Hubble tension and the puzzles of massive, UV-bright galaxies at cosmic dawn. Excitingly, forthcoming CMB experiments focused on TT and EE power spectra on small angular scales have the potential to strongly detect or exclude the presence of EDE, which will offer substantial clarity for both models of cosmology and high-redshift galaxy formation.

ACKNOWLEDGEMENTS

We thank Robert Feldmann, and Stephanie O’Neil for suggestions that improved the manuscript. MV acknowledges support through NASA ATP 19-ATP19-0019, 19-ATP19-0020, 19-ATP19-0167, and NSF grants AST-1814053, AST-1814259, AST-1909831, AST-2007355 and AST-2107724. MBK acknowledges support from NSF CAREER award AST-1752913, NSF grants AST-1910346 and AST-2108962, NASA grant 80NSSC22K0827, and HST-GO-16686, HST-AR-17028, and HST-AR-17043 from the Space Telescope Science Institute (STScI), which is operated by AURA, Inc., under NASA contract NAS5-26555. RPN acknowledges support for this work provided by NASA through the NASA Hubble Fellowship grant HST-HF2-51515.001-A awarded by STScI.

DATA AVAILABILITY

The data underlying this article can be shared on reasonable request to the corresponding author. The source code and the observational data compiled for this project are publically available at [the online repository](#).

REFERENCES

Abdalla E., et al., 2022, *Journal of High Energy Astrophysics*, **34**, 49
 Adams N. J., et al., 2023a, *arXiv e-prints*, p. [arXiv:2304.13721](#)
 Adams N. J., et al., 2023b, *MNRAS*, **518**, 4755
 Aird J., Coil A. L., Georgakakis A., Nandra K., Barro G., Pérez-González P. G., 2015, *MNRAS*, **451**, 1892
 Akins H. B., et al., 2023, *ApJ*, **956**, 61
 Akins H. B., et al., 2024, *arXiv e-prints*, p. [arXiv:2406.10341](#)
 Arvanitaki A., Dimopoulos S., Dubovsky S., Kaloper N., March-Russell J., 2010, *Phys. Rev. D*, **81**, 123530
 Atek H., et al., 2023, *MNRAS*, **519**, 1201
 Baggen J. F. W., et al., 2023, *arXiv e-prints*, p. [arXiv:2305.17162](#)
 Bakx T. J. L. C., et al., 2023, *MNRAS*, **519**, 5076
 Behroozi P. S., Silk J., 2015, *ApJ*, **799**, 32
 Behroozi P. S., Wechsler R. H., Conroy C., 2013, *ApJ*, **770**, 57
 Behroozi P., Wechsler R. H., Hearin A. P., Conroy C., 2019, *MNRAS*, **488**, 3143

Behroozi P., et al., 2020, *MNRAS*, **499**, 5702
 Bond J. R., Cole S., Efstathiou G., Kaiser N., 1991, *ApJ*, **379**, 440
 Bouwens R. J., et al., 2014, *ApJ*, **793**, 115
 Bouwens R. J., et al., 2021, *AJ*, **162**, 47
 Bouwens R., Illingworth G., Oesch P., Stefanon M., Naidu R., van Leeuwen I., Magee D., 2023a, *MNRAS*, **523**, 1009
 Bouwens R. J., et al., 2023b, *MNRAS*, **523**, 1036
 Bowler R. A. A., Jarvis M. J., Dunlop J. S., McLure R. J., McLeod D. J., Adams N. J., Milvang-Jensen B., McCracken H. J., 2020, *MNRAS*, **493**, 2059
 Boyett K., et al., 2024, *arXiv e-prints*, p. [arXiv:2401.16934](#)
 Boylan-Kolchin M., 2023, *Nature Astronomy*, **7**, 731
 Boylan-Kolchin M., Weisz D. R., 2021, *MNRAS*, **505**, 2764
 Bryan G. L., Norman M. L., 1998, *ApJ*, **495**, 80
 Bunker A. J., et al., 2023, *A&A*, **677**, A88
 Cameron A. J., Katz H., Rey M. P., Saxena A., 2023, *MNRAS*, **523**, 3516
 Carniani S., et al., 2024, *arXiv e-prints*, p. [arXiv:2405.18485](#)
 Casey C. M., et al., 2024, *ApJ*, **965**, 98
 Castellano M., et al., 2022, *ApJ*, **938**, L15
 Castellano M., et al., 2024, *arXiv e-prints*, p. [arXiv:2403.10238](#)
 Ceverino D., Nakazato Y., Yoshida N., Klessen R., Glover S., 2024, *arXiv e-prints*, p. [arXiv:2404.02537](#)
 Chaboyer B., 1995, *ApJ*, **444**, L9
 Chabrier G., 2003, *PASP*, **115**, 763
 Chworowsky K., et al., 2023, *arXiv e-prints*, p. [arXiv:2311.14804](#)
 Ciesla L., et al., 2023, *arXiv e-prints*, p. [arXiv:2309.15720](#)
 Cole J. W., et al., 2023, *arXiv e-prints*, p. [arXiv:2312.10152](#)
 Cowan J. J., Thielemann F.-K., Truran J. W., 1991, *Phys. Rep.*, **208**, 267
 Cowley W. I., Baugh C. M., Cole S., Frenk C. S., Lacey C. G., 2018, *MNRAS*, **474**, 2352
 Cueto E. R., Hutter A., Dayal P., Gottlöber S., Heintz K. E., Mason C., Trebitsch M., Yepes G., 2024, *A&A*, **686**, A138
 Cullen F., et al., 2023, *MNRAS*, **520**, 14
 Cullen F., et al., 2024, *MNRAS*, **531**, 997
 Curti M., et al., 2023, *MNRAS*, **518**, 425
 Curtis-Lake E., et al., 2023, *Nature Astronomy*,
 D’Eugenio F., et al., 2023, *arXiv e-prints*, p. [arXiv:2311.09908](#)
 Davé R., Anglés-Alcázar D., Narayanan D., Li Q., Rafieferantsoa M. H., Appleby S., 2019, *MNRAS*, **486**, 2827
 Dayal P., Ferrara A., Dunlop J. S., Pacucci F., 2014, *MNRAS*, **445**, 2545
 Dayal P., Rossi E. M., Shiralilou B., Piana O., Choudhury T. R., Volonteri M., 2019, *MNRAS*, **486**, 2336
 Dekel A., Sarkar K. C., Birnboim Y., Mandelker N., Li Z., 2023, *MNRAS*, **523**, 3201
 Desprez G., et al., 2024, *MNRAS*, **530**, 2935
 Di Valentino E., et al., 2021, *Classical and Quantum Gravity*, **38**, 153001
 Diemer B., 2018, *ApJS*, **239**, 35
 Donnan C. T., et al., 2023, *MNRAS*, **518**, 6011
 Donnan C. T., et al., 2024, *arXiv e-prints*, p. [arXiv:2403.03171](#)
 Dressler A., et al., 2024, *ApJ*, **964**, 150
 Endsley R., et al., 2023a, *arXiv e-prints*, p. [arXiv:2306.05295](#)
 Endsley R., Stark D. P., Whittler L., Topping M. W., Chen Z., Plat A., Chisholm J., Charlot S., 2023b, *MNRAS*, **524**, 2312
 Fakhouri O., Ma C.-P., Boylan-Kolchin M., 2010, *MNRAS*, **406**, 2267
 Fall S. M., Krumholz M. R., Matzner C. D., 2010, *ApJ*, **710**, L142
 Faucher-Giguère C.-A., 2018, *MNRAS*, **473**, 3717
 Feldmann R., et al., 2024, *arXiv e-prints*, p. [arXiv:2407.02674](#)
 Ferrara A., Pallottini A., Dayal P., 2023a, *MNRAS*, **522**, 3986
 Ferrara A., Pallottini A., Dayal P., 2023b, *MNRAS*, **522**, 3986
 Finkelstein S. L., et al., 2022, *ApJ*, **940**, L55
 Finkelstein S. L., et al., 2023a, *arXiv e-prints*, p. [arXiv:2311.04279](#)
 Finkelstein S. L., et al., 2023b, *ApJ*, **946**, L13
 Forconi M., Giarè W., Mena O., Ruchika Valentino E. D., Melchiorri A., Nunes R. C., 2024, *J. Cosmol. Astropart. Phys.*, **2024**, 097
 Fujimoto S., et al., 2022, *arXiv e-prints*, p. [arXiv:2211.03896](#)
 Fujimoto S., et al., 2023, *arXiv e-prints*, p. [arXiv:2308.11609](#)
 Fujimoto S., et al., 2024, *arXiv e-prints*, p. [arXiv:2402.18543](#)
 Gelli V., Mason C., Hayward C. C., 2024, *arXiv e-prints*, p. [arXiv:2405.13108](#)

- Grudić M. Y., Hopkins P. F., Faucher-Giguère C.-A., Quataert E., Murray N., Kereš D., 2018, *MNRAS*, 475, 3511
- Hainline K. N., et al., 2024, *ApJ*, 964, 71
- Harikane Y., et al., 2022, *ApJS*, 259, 20
- Harikane Y., et al., 2023, *ApJS*, 265, 5
- Harikane Y., et al., 2024a, *arXiv e-prints*, p. arXiv:2406.18352
- Harikane Y., Nakajima K., Ouchi M., Umeda H., Isobe Y., Ono Y., Xu Y., Zhang Y., 2024b, *ApJ*, 960, 56
- Harvey T., et al., 2024, *arXiv e-prints*, p. arXiv:2403.03908
- Haslbauer M., Kroupa P., Zonoozi A. H., Haghi H., 2022, *ApJ*, 939, L31
- Hegde S., Wyatt M. M., Furlanetto S. R., 2024, *arXiv e-prints*, p. arXiv:2405.01629
- Helton J. M., et al., 2024, *arXiv e-prints*, p. arXiv:2405.18462
- Hopkins P. F., et al., 2018, *MNRAS*, 480, 800
- Hopkins P. F., et al., 2023, *MNRAS*, 519, 3154
- Howlett C., Lewis A., Hall A., Challinor A., 2012, *J. Cosmol. Astropart. Phys.*, 1204, 027
- Hsiao T. Y.-Y., et al., 2023, *arXiv e-prints*, p. arXiv:2305.03042
- Inayoshi K., Harikane Y., Inoue A. K., Li W., Ho L. C., 2022, *ApJ*, 938, L10
- Iyer K. G., et al., 2020, *MNRAS*, 498, 430
- Kamionkowski M., Pradler J., Walker D. G. E., 2014, *Phys. Rev. Lett.*, 113, 251302
- Kannan R., Garaldi E., Smith A., Pakmor R., Springel V., Vogelsberger M., Hernquist L., 2022, *MNRAS*, 511, 4005
- Kannan R., et al., 2023, *MNRAS*, 524, 2594
- Karwal T., Kamionkowski M., 2016, *Phys. Rev. D*, 94, 103523
- Katz H., et al., 2023, *The Open Journal of Astrophysics*, 6, 44
- Khimey D., Bose S., Tacchella S., 2021, *MNRAS*, 506, 4139
- Klypin A., Yepes G., Gottlöber S., Prada F., Heß S., 2016, *MNRAS*, 457, 4340
- Klypin A., et al., 2021, *MNRAS*, 504, 769
- Knox L., Millea M., 2020, *Phys. Rev. D*, 101, 043533
- Kocevski D. D., et al., 2023, *ApJ*, 954, L4
- Kocevski D. D., et al., 2024, *arXiv e-prints*, p. arXiv:2404.03576
- Kokorev V., et al., 2024, *ApJ*, 968, 38
- Kragh Jespersen C., Steinhardt C. L., Somerville R. S., Lovell C. C., 2024, *arXiv e-prints*, p. arXiv:2403.00050
- Kravtsov A., Belokurov V., 2024, *arXiv e-prints*, p. arXiv:2405.04578
- Kulkarni G., Worseck G., Hennawi J. F., 2019, *MNRAS*, 488, 1035
- Labbé I., et al., 2023, *Nature*, 616, 266
- Larson R. L., et al., 2022, *arXiv e-prints*, p. arXiv:2211.10035
- Leethochawalit N., et al., 2023, *ApJ*, 942, L26
- Lewis A., Challinor A., Lasenby A., 2000, *ApJ*, 538, 473
- Li Z., Dekel A., Sarkar K. C., Aung H., Giallisco M., Mandelker N., Tacchella S., 2023, *arXiv e-prints*, p. arXiv:2311.14662
- Looser T. J., et al., 2023, *arXiv e-prints*, p. arXiv:2306.02470
- Lovell C. C., Harrison I., Harikane Y., Tacchella S., Wilkins S. M., 2023, *MNRAS*, 518, 2511
- Lu S., Frenk C. S., Bose S., Lacey C. G., Cole S., Baugh C. M., Helly J. C., 2024, *arXiv e-prints*, p. arXiv:2406.02672
- Madau P., Dickinson M., 2014, *ARA&A*, 52, 415
- Marinacci F., Sales L. V., Vogelsberger M., Torrey P., Springel V., 2019, *MNRAS*, 489, 4233
- Marsh D. J. E., 2016, *Phys. Rep.*, 643, 1
- Mason C. A., Trenti M., Treu T., 2015, *The Astrophysical Journal*, 813, 21
- Mason C. A., Trenti M., Treu T., 2023, *MNRAS*, 521, 497
- Matthee J., et al., 2024, *ApJ*, 963, 129
- Mauerhofer V., Dayal P., 2023, *arXiv e-prints*, p. arXiv:2305.01681
- McLeod D. J., McLure R. J., Dunlop J. S., 2016, *MNRAS*, 459, 3812
- McLeod D. J., et al., 2024, *MNRAS*, 527, 5004
- Menon S. H., Lancaster L., Burkhardt B., Somerville R. S., Dekel A., Krumholz M. R., 2024, *ApJ*, 967, L28
- Meurer G. R., Heckman T. M., Calzetti D., 1999, *ApJ*, 521, 64
- Mirocha J., Furlanetto S. R., 2023, *MNRAS*, 519, 843
- Mirocha J., La Plante P., Liu A., 2021, *MNRAS*, 507, 3872
- Morishita T., Stiavelli M., 2023, *ApJ*, 946, L35
- Morishita T., et al., 2018, *ApJ*, 867, 150
- Morishita T., et al., 2024, *ApJ*, 963, 9
- Moster B. P., Somerville R. S., Madau C., van den Bosch F. C., Macciò A. V., Naab T., Oser L., 2010, *ApJ*, 710, 903
- Muñoz J. B., Mirocha J., Furlanetto S., Sabti N., 2023, *MNRAS*, 526, L47
- Murray S., 2014, HMF: Halo Mass Function calculator, Astrophysics Source Code Library, record ascl:1412.006 (ascl:1412.006)
- Murray S. G., Power C., Robotham A. S. G., 2013, *Astronomy and Computing*, 3, 23
- Nadler E. O., Benson A., Driskell T., Du X., Gluscevic V., 2023, *MNRAS*, 521, 3201
- Naidu R. P., et al., 2022a, *arXiv e-prints*, p. arXiv:2208.02794
- Naidu R. P., et al., 2022b, *ApJ*, 940, L14
- Narayanan D., et al., 2024, *ApJ*, 961, 73
- Neyer M., et al., 2024, *MNRAS*, 531, 2943
- Niida M., et al., 2020, *ApJ*, 904, 89
- Oesch P. A., Bouwens R. J., Illingworth G. D., Labbé I., Stefanon M., 2018, *ApJ*, 855, 105
- Pallottini A., Ferrara A., 2023, *arXiv e-prints*, p. arXiv:2307.03219
- Pérez-González P. G., et al., 2023, *ApJ*, 951, L1
- Planck Collaboration et al., 2020, *A&A*, 641, A6
- Poulin V., Smith T. L., Grin D., Karwal T., Kamionkowski M., 2018, *Phys. Rev. D*, 98, 083525
- Poulin V., Smith T. L., Karwal T., Kamionkowski M., 2019, *Phys. Rev. Lett.*, 122, 221301
- Poulin V., Smith T. L., Karwal T., 2023, *Physics of the Dark Universe*, 42, 101348
- Press W. H., Schechter P., 1974, *ApJ*, 187, 425
- Ren K., Trenti M., Mason C. A., 2019, *The Astrophysical Journal*, 878, 114
- Riess A. G., et al., 2022, *ApJ*, 934, L7
- Robertson B. E., et al., 2023a, *Nature Astronomy*,
- Robertson B., et al., 2023b, *arXiv e-prints*, p. arXiv:2312.10033
- Rodríguez-Puebla A., Primack J. R., Behroozi P., Faber S. M., 2016a, *MNRAS*, 455, 2592
- Rodríguez-Puebla A., Behroozi P., Primack J., Klypin A., Lee C., Hellinger D., 2016b, *MNRAS*, 462, 893
- Rodríguez-Puebla A., Primack J. R., Avila-Reese V., Faber S. M., 2017, *MNRAS*, 470, 651
- Salpeter E. E., 1955, *ApJ*, 121, 161
- Shen X., Hopkins P. F., Faucher-Giguère C.-A., Alexander D. M., Richards G. T., Ross N. P., Hickox R. C., 2020, *MNRAS*, 495, 3252
- Shen X., Vogelsberger M., Boylan-Kolchin M., Tacchella S., Kannan R., 2023, *MNRAS*, 525, 3254
- Shen X., et al., 2024, *arXiv e-prints*, p. arXiv:2402.08717
- Sheth R. K., Mo H. J., Tormen G., 2001, *MNRAS*, 323, 1
- Smith T. L., Poulin V., Amin M. A., 2020, *Phys. Rev. D*, 101, 063523
- Smith T. L., Lucca M., Poulin V., Abellan G. F., Balkenhol L., Benabed K., Galli S., Murgia R., 2022, *Phys. Rev. D*, 106, 043526
- Stefanon M., et al., 2019, *ApJ*, 883, 99
- Stefanon M., Bouwens R. J., Labbé I., Illingworth G. D., Gonzalez V., Oesch P. A., 2021, *ApJ*, 922, 29
- Sugimura K., Ricotti M., Park J., Garcia F. A. B., Yajima H., 2024, *arXiv e-prints*, p. arXiv:2403.04824
- Sun G., Furlanetto S. R., 2016, *MNRAS*, 460, 417
- Sun G., Faucher-Giguère C.-A., Hayward C. C., Shen X., Wetzel A., Cochrane R. K., 2023a, *arXiv e-prints*, p. arXiv:2307.15305
- Sun F., et al., 2023b, *ApJ*, 953, 53
- Svrcek P., Witten E., 2006, *Journal of High Energy Physics*, 2006, 051
- Tacchella S., Trenti M., Carollo C. M., 2013, *ApJ*, 768, L37
- Tacchella S., Bose S., Conroy C., Eisenstein D. J., Johnson B. D., 2018, *The Astrophysical Journal*, 868, 92
- Tacchella S., Forbes J. C., Caplar N., 2020, *MNRAS*, 497, 698
- Tacchella S., et al., 2023a, *MNRAS*, 522, 6236
- Tacchella S., et al., 2023b, *ApJ*, 952, 74
- Thompson T. A., Krumholz M. R., 2016, *MNRAS*, 455, 334
- Tinker J. L., Robertson B. E., Kravtsov A. V., Klypin A., Warren M. S., Yepes G., Gottlöber S., 2010, *ApJ*, 724, 878
- Topping M. W., Stark D. P., Endsley R., Plat A., Whittler L., Chen Z., Charlot S., 2022, *ApJ*, 941, 153
- Topping M. W., et al., 2024, *MNRAS*, 529, 4087

- Trinca A., Schneider R., Valiante R., Graziani L., Ferrotti A., Omukai K., Chon S., 2024, *MNRAS*, **529**, 3563
- Umeda H., Ouchi M., Nakajima K., Harikane Y., Ono Y., Xu Y., Isobe Y., Zhang Y., 2023, *arXiv e-prints*, p. [arXiv:2306.00487](https://arxiv.org/abs/2306.00487)
- Vandenberg D. A., Bolte M., Stetson P. B., 1996, *ARA&A*, **34**, 461
- Ventura E. M., Qin Y., Balu S., Wytke J. S. B., 2024, *MNRAS*, **529**, 628
- Verde L., Treu T., Riess A. G., 2019, *Nature Astronomy*, **3**, 891
- Vogelsberger M., et al., 2020, *MNRAS*, **492**, 5167
- Wang B., et al., 2023, *ApJ*, **957**, L34
- Wang B., et al., 2024a, *arXiv e-prints*, p. [arXiv:2403.02304](https://arxiv.org/abs/2403.02304)
- Wang B., et al., 2024b, *ApJ*, **963**, 74
- Weibel A., et al., 2024, *arXiv e-prints*, p. [arXiv:2403.08872](https://arxiv.org/abs/2403.08872)
- Wilkins S. M., et al., 2023a, *MNRAS*, **518**, 3935
- Wilkins S. M., et al., 2023b, *MNRAS*, **519**, 3118
- Winget D. E., Hansen C. J., Liebert J., van Horn H. M., Fontaine G., Nather R. E., Kepler S. O., Lamb D. Q., 1987, *ApJ*, **315**, L77
- Xiao M., et al., 2023, *arXiv e-prints*, p. [arXiv:2309.02492](https://arxiv.org/abs/2309.02492)
- Yan H., Ma Z., Ling C., Cheng C., Huang J.-S., 2023, *ApJ*, **942**, L9
- Ying J. M., Chaboyer B., Boudreux E. M., Slaughter C., Boylan-Kolchin M., Weisz D., 2023, *AJ*, **166**, 18
- Yung L. Y. A., Somerville R. S., Finkelstein S. L., Popping G., Davé R., 2019, *MNRAS*, **483**, 2983
- Yung L. Y. A., Somerville R. S., Nguyen T., Behroozi P., Modi C., Gardner J. P., 2024a, *MNRAS*,
- Yung L. Y. A., Somerville R. S., Finkelstein S. L., Wilkins S. M., Gardner J. P., 2024b, *MNRAS*, **527**, 5929
- Zavala J. A., et al., 2023, *ApJ*, **943**, L9
- Zavala J. A., et al., 2024, *arXiv e-prints*, p. [arXiv:2403.10491](https://arxiv.org/abs/2403.10491)
- Zhang E., et al., 2024, *arXiv e-prints*, p. [arXiv:2406.10338](https://arxiv.org/abs/2406.10338)
- de Graaff A., et al., 2024a, *arXiv e-prints*, p. [arXiv:2404.05683](https://arxiv.org/abs/2404.05683)
- de Graaff A., et al., 2024b, *A&A*, **684**, A87

This paper has been typeset from a $\text{\TeX}/\text{\LaTeX}$ file prepared by the author.